ACS APPLIED NANO MATERIALS

www.acsanm.org Article

Nanoporous Silica–Alumina Films Fabricated on Silicon Photonic Chips for Selective Ammonia Sensing

Yanlu Li, Claudio Bellani, Nebiyu Yebo, Jolien Dendooven, Jin Won Seo, Christophe Detavernier, Roel Baets, Johan A. Martens, and Sreeprasanth Pulinthanathu Sree*

Cite This: *ACS Appl. Nano Mater.* 2022, 5, 16126–16135 Read Online

ACCESS | Metrics & More | Article Recommendations

ABSTRACT: Surface-modified nanoporous silica films offer attractive features for analyte-specific gas detection applications. Here we demonstrate the integration of highly porous silica–alumina films on silicon nanophotonic chips and their performance in selective NH_3 detection. Prototype sensors with microporous as well as mesoporous silica films were assembled. The incorporation of aluminum in trace amount needed to generate acid sites was achieved during film deposition or using postsynthesis atomic layer deposition. Silicon photonic micro-ring resonators functionalized with both techniques demonstrated a selective response to NH_3 relative to CO_2. Furthermore, the response was rapid and reversible. The role of preadsorbed water vapor on the reversible nature of the sensor is also investigated. Experimental observations indicate that water vapor preadsorbed on the films leads to fast sensor recovery while maintaining selectivity toward NH_3. This could be attributed to the relatively less strong and still selective binding of NH_3 on protonated water molecules preadsorbed on the surface acid sites. The potential of modified nanoporous films for portable and low-cost NH_3 sensing on optical chips demonstrated here can be exploited in health care as well as industrial applications.

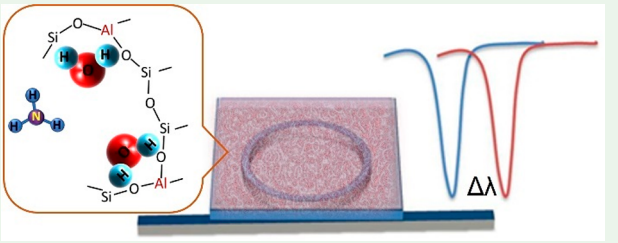

KEYWORDS: *nanoporous silica films, micro-ring resonators, atomic layer deposition, selective gas sensing, ammonia detection*

INTRODUCTION

Nanoporous thin films with accessible porosity are of interest to many applications including the development of adsorptive surfaces for optoelectronic sensor devices.[1−7] Particularly, nanoporous silica and aluminosilicate films with transition metal oxide nanoparticles deposited on optical waveguide structures have been shown to be attractive for optical sensing.[8,9] Adsorption of even trace amounts of gaseous or liquid analytes alters the refractive index or optical absorption of nanoporous coatings, hence making these planar optical systems suitable for sensing.[10−12] A large surface area and accessible porosity in the sensor film can lead to high sensitivity to guest molecules. In addition, modification of nanoporous silica surfaces by introducing functional groups can enable analyte-specific detection which is needed in the majority of environmental, industrial, and medical applications. Chemical functionality can be introduced either during synthesis or via postsynthesis modification.[13] Atomic layer deposition (ALD) is a self-limiting thin film growth technique where a substrate is subjected to sequential exposures of chemical precursors and has been demonstrated to be an efficient postsynthesis functionalization technique for mesoporous films.[14,15]

Among other optical technologies, ultracompact and CMOS-compatible silicon nanophotonic planar sensors are emerging as promising technology for highly portable and low-cost sensing applications.[10,11,16−20] Using CMOS fabrication technology, inexpensive mass fabrication along with seamless integration in a portable footprint can be achieved. Moreover, these miniature sensors can easily be multiplexed for parallel detection of gas mixtures on a photonic chip.

One of the silicon photonic components promising for gas sensing applications is a micro-ring resonator (MRR). MRRs are resonant structures with a typical diameter of only several micrometers on an optical chip. The resonant behavior of these structures shows a high sensitivity to physical changes in the surrounding, making them attractive as miniature sensors.[10,11,16−20] MRRs offer inherent multiplexing features for straightforward sensor array implementation. An optical micro-ring resonator is a ring waveguide cavity coupled to access waveguides. Light is coupled in and out of the ring waveguide using the straight access waveguides. An MRR supports circulating resonant waveguide modes. The electric

Received: June 23, 2022
Accepted: October 17, 2022
Published: October 27, 2022

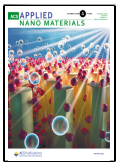

field of these guided modes extends to the surface of the ring allowing evanescent field interaction with the outside environment. Particularly, high index contrast waveguide structures such as silicon-on-insulator (SOI) MRRs presented here are characterized by strong evanescent field localized at the waveguide surfaces. As a result, high sensitivity to variations in the surrounding refractive index can be achieved. For each MRR, there is a series of resonance wavelengths. Light with these wavelengths is enhanced within the ring which leads to enhanced absorption or scattering relative to nonresonant wavelengths. Therefore, a transmission dip can be found in the through-port of the MRR (Figure 1). The corresponding

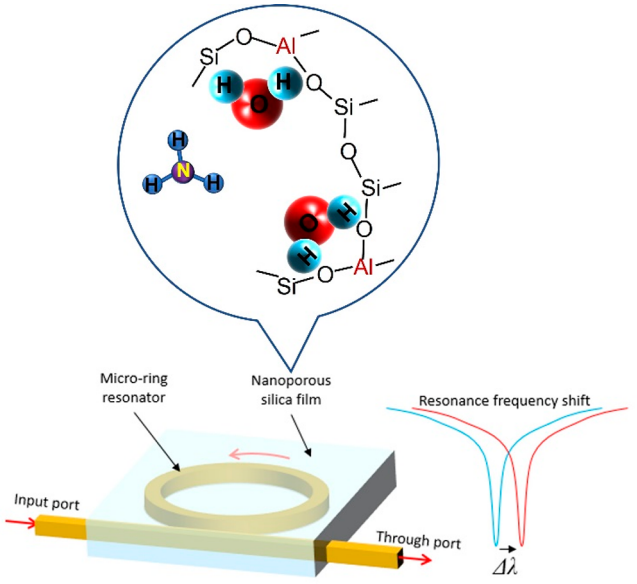

Figure 1. Alumino slicate functionalized micro-ring resonator (MRR) in ammonia sensing and effective index change induced resonance shifts.

resonance shift $\Delta\lambda$ in the micro-ring resonance wavelength can be estimated by eq 1,

$$\frac{\Delta\lambda}{\lambda} = \frac{\Delta n_{\text{eff}}}{n_g} \tag{1}$$

where λ, n_{eff}, and n_g represent the resonance wavelength, the effective index, and the group index of the guided mode, respectively. The resonance shift can be spectrally quantified as a measure of the concentration of a given analyte being detected. Figure 1 sketches a surface-functionalized MRR and resonance shift due to changes in the surroundings.

Adsorption of NH_3 molecules onto the surface of these nanoporous films leads to an effective index change of the coated ring resonator. The effective index change can be attributed to a combination of physical mechanisms including pore-filling, adsorption, heat, and change in carrier density of the film.[11,16,21,22] An increased density of guest molecules in the porous films can change the film refractive index. On the other hand, since adsorption is an exothermic process, the resulting heat of adsorption can alter the effective index via the thermo-optic effect.[10,21] Moreover, charge exchange between surface sites and guest molecules can modify the carrier density and hence the film refractive index.[22] The predominant mechanism behind the capacity of these aluminosilicate materials for selective uptake of NH_3 has been explained by studying a powder counterpart of the material using advanced NMR techniques.[23] It was evident from the study that a majority of ammonia is blended with the hydrogen-bonded water network in the micropores of the aluminosilicate as indicated in Figure 1.

There exists different materials which can sense ammonia, but there are challenges associated with them while in application. For example metal oxide semiconductors[24−27] are highly sensitive and cheap but their high operating temperature, water sensitivity, long recovery period, and poor selectivity in complex gas mixtures are some drawbacks in using them for ammonia sensing. Conducting polymers[24,28−30] are highly selective and fast in ammonia sensing, but their low reproducibility and low stability are issues. While non-conducting polymers[24,31] can operate at low temperatures, their poor stability and selectivity make them less attractive. Metal organic frameworks, MOFs,[32,33] are highly selective and sensitive but demand of crystalline structure to exhibit sensitivity and water sensitive nature of many MOFs are challenges in using them for ammonia sensing. Carbon nanotubes[28,34−38] and graphene[33,39,40] possess high sensitivity and can operate at low temperatures, but their costs, low recovery times, and difficulties in transferring it to the desired form are challenges. Aluminosilicates especially in the form of thin films are more interesting as they are stable, highly sensitive, reproducible, and cheap and have high adsorption capacity due to high surface area. Note that the MRR is not the only sensing structure to detect the refractive index change of microporous coating layers. Other photonic structures, e.g., Mach−Zehnder interferometers (MZIs) and various other whispering gallery mode (WGM) sensors,[41] are also often used. One example is a silicon nitride MZI covered with a mesoporous silica layer, which has demonstrated ppb level sensitivities to acetone, isopropyl alcohol, and ethanol.[12] The other example is different kinds of WGM sensors, which take advantage of the WGM formed by the outer boundary of a circular cavity. The cavities can be microtoroid, microdisk, microsphere, microbottle, and microbubble.[41] In many cases, MRRs are considered as WGM sensors. But in this paper, the name "WGM sensor" indicates those WGM sensors which are different from the MRRs. Many reported WGM sensors have much smaller optical losses than those in MRRs. One reason is that the optical fields in a (single-TE-mode) MRR sensor experience side-wall scattering from both sides of the waveguide, while that scattering effect only happens on one side of a WGM sensor. Additionally, most reported WGM sensors are thermally treated (e.g., laser reflow[42]) in the fabrication process to enable an atom-scale surface roughness at the boundary of the WGM sensor. As a result, most reported WGM sensors have very low optical losses and very high quality-factors (Q-factors), e.g., 100 million.[42,43] In comparison, untreated MRRs usually have Q factors between 10^4 and 10^6.[11,44,45] A WGM based ammonia sensor having high sensitivity with parts-per-trillion level limit of detection has been reported recently.[46] But the disadvantage of WGM sensors is the high fabrication cost associated with the special surface treatments. Though MRR sensors generally have worse Q factors, their sensor sensitivities (resonance wavelength shift per refractive index change of the cladding material) can be better since they can interact with the sensing material from both sides.[47] What's more, the choice of the Q factor also depends on the wavelength resolution of the tunable laser source. The laser wavelength resolution in our system is 10 pm,

https://doi.org/10.1021/acsanm.2c02741
ACS Appl. Nano Mater. 2022, 5, 16126−16135

which fits well with the full-width at half-maximum (FWHM) of the MRR resonances (around 110 pm). This resolution is not good enough to detect the resonance of a high-Q WGM sensor.

Despite the considerable benefits ultracompact optical sensors can offer, progress in the integration of highly sensitive and analyte-specific materials is yet to be made to fully exploit their potential. The authors previously demonstrated the feasibility of integrating aluminosilicate films with MRRs and selective detection of ammonia.[11] In the present study, we investigate the sensitivity limits and the interference of other gases (e.g., CO_2) and molecules (e.g., water and acetone). The performance repeatability of the sensor is also studied concerning applications where the sensor is exposed continuously to ambient conditions.

For creating Al functionalized coating over MRRs two approaches are used. The first technique involves the incorporation of aluminum during the synthesis of microporous silica films, whereas in the second approach, spacious mesoporous silica films are initially prepared on the sensor chips and afterward functionalized by atomic layer deposition of aluminum. Al content in these films imparts acidic surface sites favorable for NH_3 adsorption. We achieved selective, fast, reversible, and durable ammonia detection using nanophotonic chips coated with both types of aluminosilicate films

EXPERIMENTAL SECTION

Fabrication of MRRs. The MRR in SOI used as the substrate for casting nanoporous films had a radius of 5 μm and was designed for operation in the telecom wavelength band near 1550 nm. The bus and ring waveguides are 220 nm high and 450 nm wide in dimension. For coupling light in and out of the rings, grating couplers are connected to the bus waveguides through adiabatic tapers. The distance between the two grating couplers is ~3.5 mm. This long separation is chosen to reduce the amount of optical power coupled from the input port to the output ports directly via the bottom of the chip. An array of MRR channels is designed in such a way that the input and output grating couplers are placed close to each other so that they can be illuminated at the same time when the light source is placed at a certain distance away from the chip (Figure 2). In practice, two MRRs were placed on

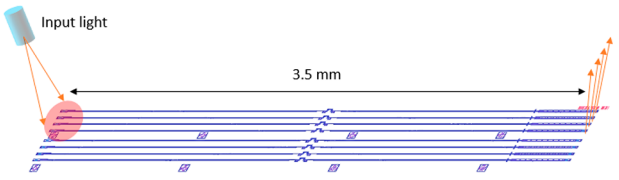

Figure 2. Schematic of the MRR biosensors and the method to couple light into the sensors.

each bus waveguide to evaluate the Vernier effect. However, in this paper, we still use the resonance shift of a single ring for sensing. The silicon photonic chips are fabricated using standard CMOS fabrication tools. The standard fabrication process starts with wafer-scale photoresist patterning of silicon-on-insulator substrates with 193 nm deep-UV lithography.[48] After this step, nanophotonic structures are formed by dry etching the top 220 nm thick silicon layer. The SOI substrate consisted of a 2 μm thick buried oxide layer sandwiched between a top silicon layer and a bottom silicon substrate.

Microporous Aluminosilicate Film Deposition on MRR. The preparation of microporous films starts with the synthesis of Clear Solution containing silica nanoslabs doped with Al. To introduce Al, Al powder was dissolved in an aqueous tetrapropylammonium hydroxide (TPAOH) aqueous solution. Tetraethylorthosilicate (TEOS) was added and hydrolyzed, and subsequently, water was added. The final molar ratio of TEOS/Al/TPAOH/H_2O was 25:0.25:9:400. An amount of 2 mL of the resulting clear solution was diluted with 8 mL of absolute ethanol and spin-coated on the SOI samples. Afterward, the films on the silicon MRRs were kept in a hydration chamber with constant humidity (75%) for a day and then dried at 60 °C followed by calcination at 350 °C with a heating ramp of 0.5 °C/min.

Mesoporous Silica Film Deposition on MRR. The synthesis of mesoporous silica thin films was adapted from ref 49. In a typical preparation, initially a colloidal suspension of silica nanoslabs called "Clear Solution" was prepared by hydrolysis of TEOS in aqueous TPAOH solution followed by addition of water. After adding H_2O, the clear solution was kept stirring for 24 h. The molar ratio of TEOS/TPAOH/H_2O was 25:9:400. 4.5 g of this suspension was mixed with 2.25 g of 5 M HCl and then combined with 6 g of 10% (wt) aqueous Pluronic P123 triblock copolymer (EO20PO70 EO20) solution which was already acidified using 2 g of 5 M HCl. 2 ml of the resulting suspension of the nanoslabs and the triblock copolymer was diluted with 8 mL of absolute ethanol and spin-coated on the SOI samples. Then the films were hydrothermally annealed at 90 °C for ~60 h by suspending them in an autoclave filled with water at the bottom. After drying at 60 °C, the films were calcined at 350 °C using a slow heating ramp of 0.5 °C/min.

Al-ALD to the Mesoporous Silica Films on Si MRRs. Al ALD into the mesoporous silica films integrated onto the Si MRRs was done in a home-built ALD reactor. The chemical precursors used in ALD were trimethylaluminum (TMA) and water. For the sensors studied in this work, 10 ALD cycles were performed where each cycle involves two subsequent self-terminating half-reactions. In the first half-reaction, the sample is exposed to TMA [$Al(CH_3)_3$, 97% purity, Sigma-Aldrich] for 10 s, followed by a 15 s evacuation of the reaction chamber. The second half-reaction consists of a 10 s water pulse, again followed by a 15 s evacuation. The depositions were done at a temperature of 200 °C at a pressure of TMA and H_2O vapor of 0.3 Pa.

Ellipsometric Porosimetry (EP). EP on the calcined film was carried out in a vacuum chamber to which the spectroscopic ellipsometer (Sentech SE801, 350−850 nm wavelength) was mounted and a system for dosing adsorbates was connected. The probe molecule used was toluene. For the recording of the adsorption−desorption isotherms, the adsorbate pressure was slowly increased until the saturation pressure was reached followed by slow evacuation of the chamber. The ellipsometric angles Ψ and Δ over the whole spectral range of 350−850 nm, the pressure, and the time were continuously recorded. These data were used for the calculation of porosity and pore size distribution as described in literature.[49,50]

High resolution transmission electron microscopy (HR TEM) was performed with a probe-corrected transmission electron microscope (ARM200F cold-FEG, JEOL) operated at an acceleration voltage of 200 kV. The samples were prepared by dispersing the patches of film scrapped off from a silicon wafer in 2-propanol and placing a few drops of the suspension onto the copper TEM grids covered with a lacey carbon film (Pacific Grid Tech).

HR-SEM was performed on a Nova NanoSEM450 (FEI) scanning electron microscope. The films casted on silicon wafers were mounted on Al stubs using carbon stickers and observed without any additional coating, using low voltages and a concentric backscattered (CBS) detector in the immersion lens mode.

Sensing Measurement. The sensitivity experiments were done in an optical setup equipped with a small gas chamber, a tunable laser, and an infrared (IR) camera (Figure 3a). The sensor chip is kept in the chamber which is sealed on top by a glass window. The glass window allows vertical light coupling in and out of the sensor chip via grating couplers. At the input side, a single-mode fiber is used to couple light from the tunable laser (Santec TSL-510) with an optical power of 2 mW and wavelength tuning resolution of 10 pm. The output light beams from the sensor chip are collected by an IR camera (Xenics-Xeva), while the laser is tuned across the resonance wavelength with a range of 5 nm (Figure 3b). Because of the distance between the input fiber and the input grating couplers, light

https://doi.org/10.1021/acsanm.2c02741
ACS Appl. Nano Mater. 2022, 5, 16126−16135

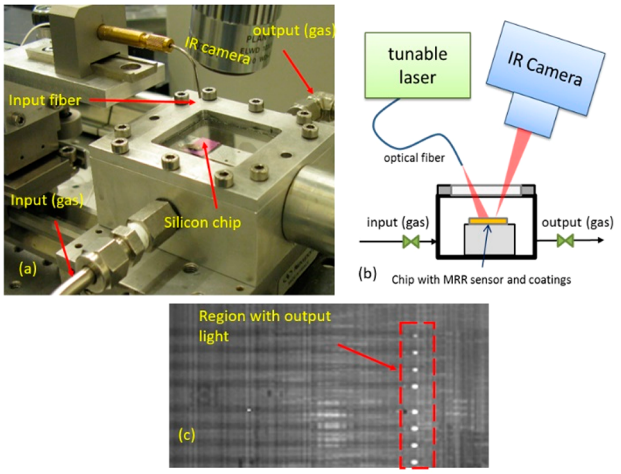

Figure 3. (a) Measurement setup to test the sensitivity of coated MRRs to gases. (b) Schematic of the setup. (3) IR image of the output grating couplers, in which the bright spots on the grating couplers only shine when the input light is coupled into the MRR via the input grating couplers

can be coupled to several waveguides with different MRRs simultaneously. The transmission signals of these MRRs can then be picked by the IR camera from the corresponding output grating couplers. (Figure 3c). The wavelength data from the tunable laser source and the intensity data from the camera are sent to a data acquisition card simultaneously. Therefore, we can retrieve the output spectra from the MRRs at each sweep cycle (around 9 s).

The measured full-width at half-maximum (fwhm) value of the transmission of the MRRs coated with microporous film is around 110 ± 10 pm, which corresponds to a *Q*-factor of around 13 900 at 1530 nm. The measured free spectral range (FSR) is around 13.4 nm, which is much larger than the wavelength tuning range in the measurement (5 nm). The extinction ratios of the coated MRRs are between 4.5 and 11 dB. This deviation is mainly associated with the different local properties of the deposited film on different MRRs. The optical properties of the MRRs will change after the coating, which is however not studied in this paper.

Streams of NH_3 gas from storage cylinders are diluted with pure N_2 by using mass flow controllers (MFCs) from Bronkhorst and introduced at different concentration levels into the test chamber. While changing the gas concentration, the total flow rate is kept constant at 100 L/h or 200 L/h. Since the target application is breath analysis, the responsivities to NH_3 are measured when CO_2 and H_2O are also present in the same gas. The H_2O is added by sending a fraction of N_2 flow through a bubbler filled with water. A schematic diagram of the gas control system is shown in Figure 4.

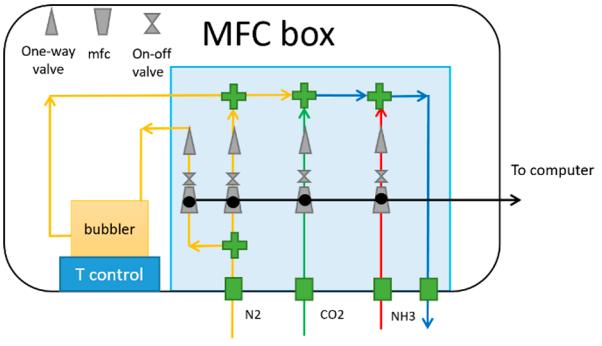

Figure 4. Schematic of the gas control system based on MFCs.

RESULTS AND DISCUSSION

The calcined microporous aluminosilicate films on the silicon MRRs were ~100 nm thick. The toluene adsorption isotherm determined using EP (Figure 5) shows very strong toluene

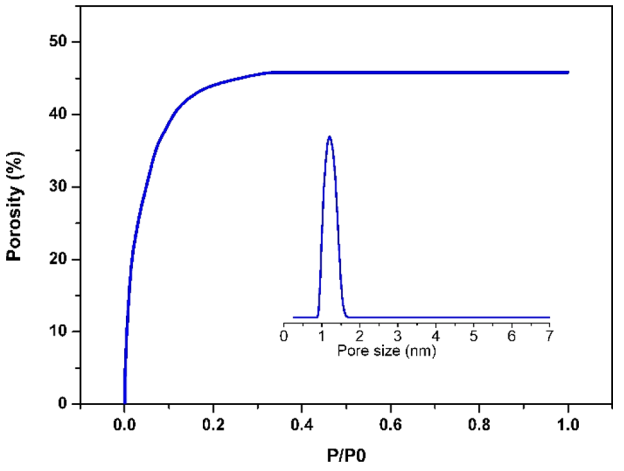

Figure 5. Adsorption isotherm and corresponding micropore size distribution (inset) measured by EP on a calcined microporous silica−alumina film similar to one coated over the MRR.

uptake at low relative pressure, due to strong adsorption in micropores. The absence of hysteresis revealed that the films were purely microporous. The pore size distribution calculated from the adsorption branch was centered at 1.2 nm. The microporous films with 100 nm thickness processed a low refractive index of 1.2 and a porosity of ~45% which is quite high for a microporous film specimen. Similar measurements on a mesoporous film present an isotherm with a clear hysteresis loop between the adsorption and desorption branches in the P/P° range 0.4−0.8 revealing the presence of mesopores. The porosity was ~70% and the distribution of pore diameters centered around 7 nm (Figure 6). The high porosity is the reason for the very low refractive index of 1.09 for these films. The film thickness was around 120 nm. HR SEM of microporous films cast on a plain silicon wafer

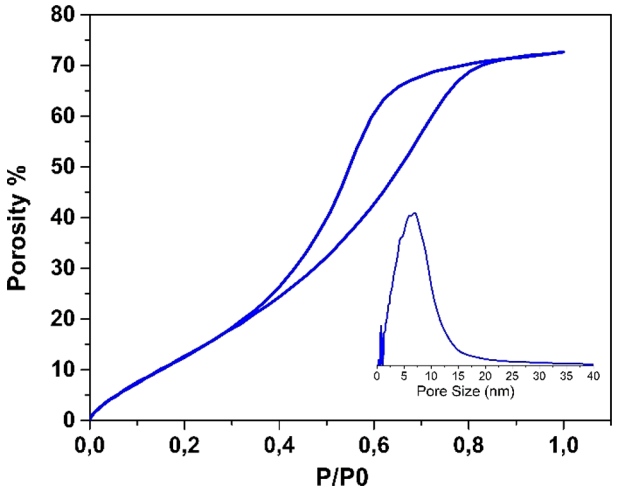

Figure 6. Toluene adsorption isotherms measured by ellipsometric porosimetry (EP) and mesopore size distribution (inset) of a calcined silica film which is representative of the mesoporous silica coating over the MRR prepared for further functionalization with Al ALD.

https://doi.org/10.1021/acsanm.2c02741
ACS Appl. Nano Mater. 2022, 5, 16126−16135

presented a very smooth surface whereas in the case of mesoporous films randomly ordered pores can be visualized from the surface itself (Figure 7a,b). HR TEM performed on

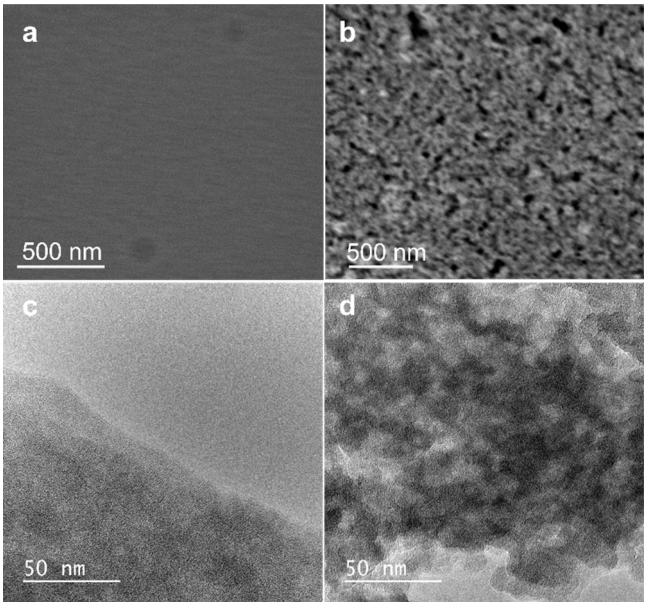

Figure 7. (a, b) HR SEM and (c,d) HR TEM of microporous and mesoporous films, respectively.

patches of films scrapped off from the thin film made on a silicon wafer revealed similar random porous network (light gray and white areas). As expected, microporous film are denser than mesoporous ones (Figure 7c,d).

For sensitivity of microporous layers on MRRs, the responsivities of the MRRs coated with the microporous aluminosilicate films to different NH_3 concentrations have been measured. The NH_3 concentrations are set as 100 ppb, 250 ppb, 500 ppb, and 1.25 ppm by the MFCs, while the flow rate is kept at 200 L/h. The humidity of the gas is set to 80% at 20 °C to get a similar condition as the respiratory gas. For each test period, the gas with the desired NH_3 concentration is sent to the chamber for 5 min. Then NH_3 flow is stopped. Meanwhile, the sample is blown by pure N_2 for another 10 min to drive out the residual gas. The gas flows with the same NH_3 concentration are repeated three times before changing the NH_3 concentration. During the measurement, the tunable laser repeats the sweep of its output wavelength while the IR camera is reading the corresponding output spectrum from the grating couplers. Each sweeping period is around 9 s. Before the entire measurement is started, the sample is baked on a hot plate at 150 °C. The baking process can drive any residual gas out of the pores and hence regenerate the MRRs.

Four MRRs from four adjacent grating couplers were measured. The relative wavelength shifts of the MRR resonance wavelengths are calculated from the obtained spectra. One example of the output spectra is shown in Figure 8. It can be seen that the resonance frequencies of these transmission spectra can be distinguished. However, their extinction ratios (ERs) (between 4.5 and 11 dB) and Q factors (around 13 900) are not very high. One reason is that the MRR waveguide is designed in such a way that a large portion of the optical field is outside of the waveguide core to sense the adsorbed gas. This design improves the sensitivity of the MRR but also increases the scattering loss of light and hence reduces

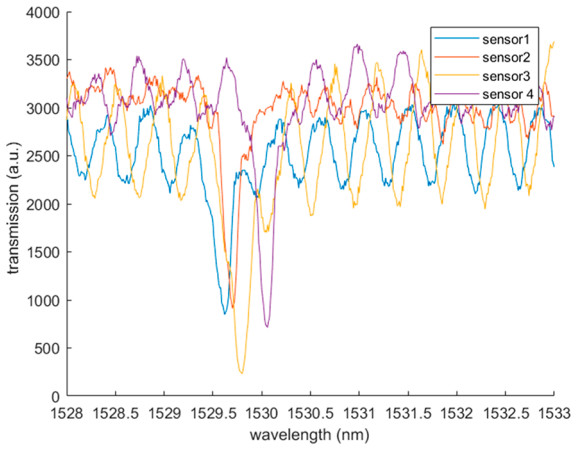

Figure 8. Through port spectra for the four MRRs, showing the resonance dips.

the Q-factors and the ERs. There are relatively strong ripples in the spectrum, which are caused by another cavity in the system. Based on the free spectrum range of the ripples, it could be inferred that they are originating from the interference between the grating coupler and the bottom of the PIC (thickness of the PIC is ~750 μm). These ripples can also shift as a result of temperature change, which will hence impact the resolution of the retrieved resonance wavelengths.

To obtain the resonance wavelength with relatively good accuracy, we first obtain the minimal value of the transmission dip λ_{min}. Then a mass-center algorithm is applied to the range of $[\lambda_{min} - 15\ pm, \lambda_{min} + 15\ pm]$, while the spectra outside of this range are all set to zero. The mass center of the transmission dip is obtained by calculating the value of $\lambda_{mc}(t) = \sum T_r(\lambda,t)^4 \cdot \lambda / \sum T_r(\lambda,t)^4$, where $T_r(\lambda,t) = T_{trans}(\lambda,t) - T_{trans,max}(t)$, $T_{trans}(\lambda,t)$ is the transmission at wavelength λ, and $T_{trans,max}(t)$ is the maximal transmission value in the entire spectrum. The power of the fourth was used in the calculation to ensure that the contribution of the dip has the greatest impact on the calculated value. Then the change of the "mass center" $\lambda_{mc}(t)$ is assumed to equal the shifts of the resonance wavelength.

The resonance wavelength shifts of the four MRRs as a function of time are shown in Figure 9. It can be seen that the wavelength responses of sensors 2, 3, and 4 are very similar, while sensor 1 is different from the others. The deviation of sensor 1 from the other sensors can be explained by the lower ER of the corresponding resonance dip and the higher fringes in the transmission spectrum (Figure 8).

In the experiments, no temperature controller is used in the setup to avoid the small temperature variations induced by a temperature controller. As a result, the wavelength will drift slowly due to the change of the temperature, but this effect can be removed in software. In these experiments, the slow wavelength drift is retrieved from a number of data points that should be very similar when there is no tempeature drift. In practice the data points just before each NH_3 pulses are used. These data are then fitted to a fourth-degree polynomial, which are then subtracted from the original data to obtain the data shown in Figure 9. The order of fourth degree is an empirical value that ensures the best polynomial fitting to the measured data. Another option is to use a reference temperature sensor (e.g., an MRR without any coating), which however requires extra processes (such as photolithography and lift-off) that may

https://doi.org/10.1021/acsanm.2c02741
ACS Appl. Nano Mater. 2022, 5, 16126−16135

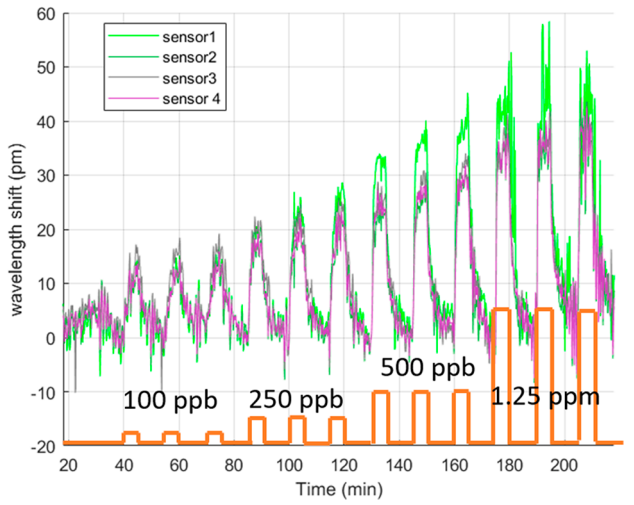

Figure 9. Resonance wavelength shifts as a function of time for four adjacent MRR sensors. The corresponding NH_3 concentrations set by the MFC are also plotted in the same figure.

change the performance of the nanoporous coatings by leaving residue materials. Therefore, we did not make reference temperature sensors for these measurements.

The ER of a channel was also evaluated from the mass-center algorithm by using the total mass of the spectrum. A smaller mass $(=\sum T_r(\lambda,t)^4 \cdot \lambda)$ means a smaller ER, hence a worse signal quality. The weighted average of $\lambda_{mc}(t)$ over all four sensors could be calculated, we use the mass as the weight factor for the averaging. Therefore, the spectra with smaller ERs have less contribution to the averaged results. The averaged wavelength responses to the NH_3 are shown in Figure 10. We can see that the averaged responses are closer to the

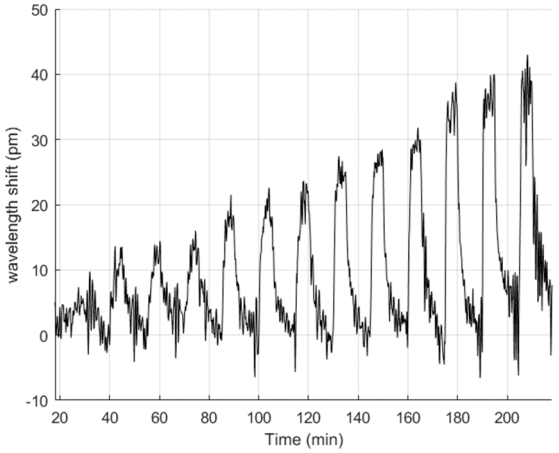

Figure 10. Averaged resonance wavelength shifts as a function of time with a relative humidity of 80% at 20 °C.

values of sensors 2, 3, and 4. The contribution of sensor 1 signals (the green curve in Figure 9) to these average values is small because of the low ER in the sensor 1 signals.

As mentioned, in total three test pulses for each NH_3 concentration were used, which can also be averaged. The averaged response curves for the tested NH_3 concentrations are shown in Figure 11. It can be seen that the rise times are different for different NH_3 concentrations. A higher NH_3 concentration corresponds to a faster rise time. For 1.25

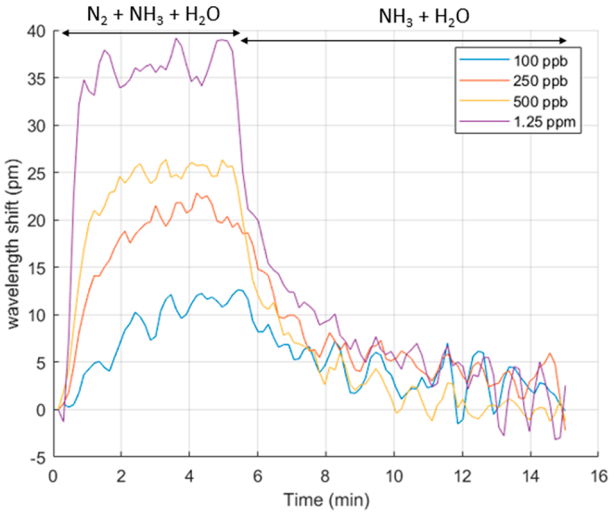

Figure 11. Time responses of the resonance wavelength of the MRRs as functions of time for different NH_3 concentrations with a relative humidity of 80% at 20 °C.

ppm concentration, it takes only around 30 s to reach 95% of the peak value. For 100 ppb concentration, the rise time is ~4 min. The average recovery time from the maximal resonance shift to 5% of the maximal resonance shift for these samples is a bit longer than 8 min, which is longer than our previous demonstration.[11] The main reason is that the NH_3 concentrations demonstrated in this paper are much smaller. But it is already much faster than other techniques.[51,52]

It can be seen that the MRR resonators with microporous layers are good enough to detect ppb levels of NH_3 with relative humidity (RH) of 80%. The response can be detected within 5 min. The wavelength shift response for 100 ppb NH_3 concentration is greater than 10 pm. The noise amplitude is estimated by calculating the difference between 10% and 90% percentiles of the resonance shift values in the last 3 min in each period, which is around 6 pm. The four sensors experience correlated noise which may be induced by temperature change or flow rate change (due to the existence of the bubbler that is used for controlling the RH). Therefore, averaging these four sensors will not reduce the major noise. However, averaging over the three successive pulses in one measurement can suppress the noise and make the 10−90% amplitude of the noise go down to ~3.5 pm. For the NH_3 pulse with 1.25 ppm concentration, the response is between 35 and 40 pm. The responses were measured twice, and the corresponding response curves are shown together in Figure 12. It can be seen that the responsivity deviations between two different measurements are usually less than 5 pm. In these measurements, the samples are cleaned and regenerated on a hot plate in the open air. After regeneration, the sample is transported to the measurement chamber, during which some H_2O or other gases may be absorbed into the microporous layer. As a result, the initial status of the MRRs can be different from time to time. A prebaking step inside the chamber may help to further clean the microporous layer. We tested the responsivities of the MRRs to NH_3 with the prebaking steps. The prebake temperature was set at 40 °C, and the prebaking time was 10 min. The corresponding NH_3 responses are also shown in Figure 12. It is seen that the NH_3 responses were generally higher than those without prebaking steps, and their relative deviations were also smaller (<3 pm).

https://doi.org/10.1021/acsanm.2c02741
ACS Appl. Nano Mater. 2022, 5, 16126−16135

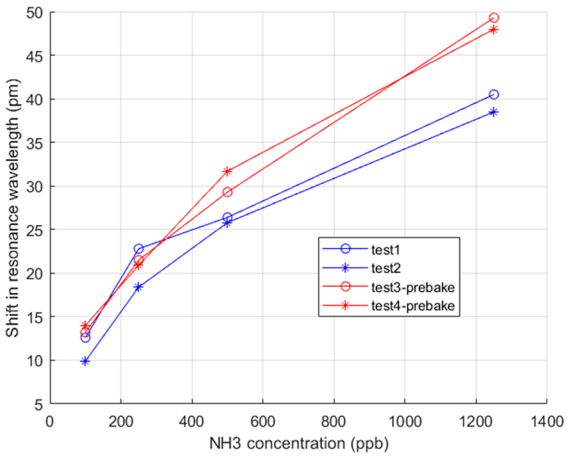

Figure 12. Resonance wavelength responses to different NH_3 concentrations. The blue curves are two repeated measurements on one MRR chip, while the red curves stand for the responsivities of the MRR chips with a prebaking step. The relative humidity is 80% at 20 °C.

We noticed that the MRRs are very sensitive to H_2O. The measured responsivity to different RH (no NH_3) at 20 °C is shown in Figure 13. It can be seen that the response to RH change is very strong. Therefore, it is important to control the relative humidity for NH_3 sensing.

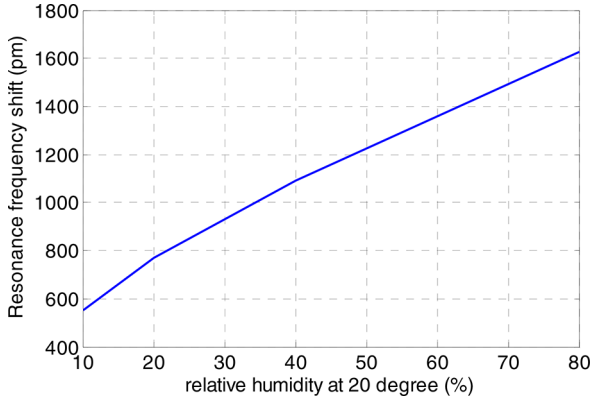

Figure 13. Resonance wavelength shifts as a function of relative humidity at 20 °C. The measurements were done in conditions without any NH_3 gas.

The responsivities for different NH_3 concentrations in dry conditions are slightly higher than those in the condition with RH = 80%. The responsivity curves to NH_3 pulses at a dry conditions are shown in Figure 14. In these measurements, we did not introduce any H_2O in the gas. However, there was still a very small amount of H_2O introduced from the tube system during the measurements. Therefore, the term "very low relative humidity" is used to describe this condition. Note that the used NH_3 concentrations for the "very low relative humidity" are different from those used with RH = 80%. That is because different mass controllers were used for these two cases. It is also found that the curves of the responses in the dry condition have weaker fluctuations compared to the measured signals in the RH = 80% condition. That may be related to not using the bubbler, which may cause an unsteady flow rate and varying H_2O concentrations.

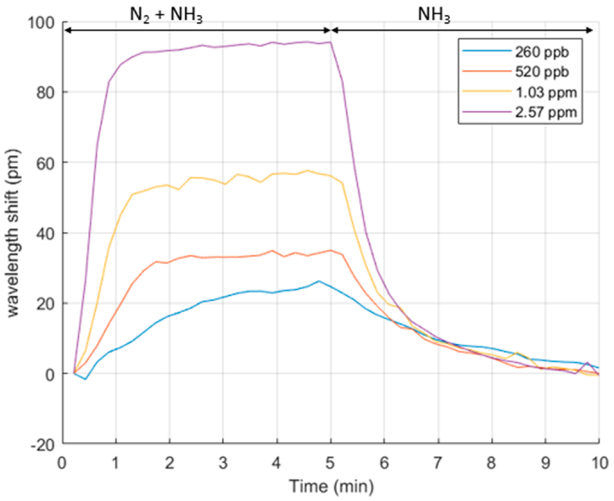

Figure 14. Time responses of the resonance wavelength of the MRRs as a function of time for different NH_3 concentrations with a very low relative humidity at 20 °C.

In normal breath, there is also a relatively large concentration of CO_2, which can impact the NH_3 responsivity. We tested the MRR responses to different NH_3 concentrations in a condition with 0.8% of CO_2 (RH = 80%). It was found that the response of the MRR to 250 ppb NH_3 is around 22.8 pm, while to 500 ppb NH_3 the response was 27 pm. These values are within the error range of the NH_3 responses when no CO_2 exists. After the CO_2 concentration was changed from 0 to 1.6%, the MRR's response to NH_3 was not clearly changed. Therefore, we can conclude that the presence of CO_2 does not impact the measurement of NH_3 at the condition of RH = 80%. However, in a drier condition, CO_2 can also introduce a relatively large shift in the MRR sensor. For example, 1% CO_2 can cause a shift of 60−70 pm. But when H_2O is present (RH = 80%), the impact of CO_2 on MRR will be strongly reduced.

Additionally, the response of MRRs to NH_3 with the presence of acetone was also tested. With 100 ppm acetone, the response of NH_3 does not change significantly from the case without acetone. So, it can be understood that the presence of acetone does not impact the MRR's response to NH_3. However, the change in acetone concentration does lead to a change in the MRR resonance, which is shown in Figure 15. It is also found that when no H_2O is present, the response to acetone is much stronger.

Besides the microporous layer, the mesoporous layer which has relatively larger pore sizes was also tested. By introducing acidic functional material (Al) into the mesoporous material, it can also be used for sensing NH_3 gas. One example is shown in Figure 16. The mesoporous layer has a pore size of around 7 nm. They are functionalized with Al_2O_3 by 10-cycle ALD. The relative humidity of the gas in these measurements is 80%. The flow rate was set as 100 L/h to reach a higher NH_3 concentration. It turned out that the mesoporous layers also have a ppb-level LOD. However, since the measurements were done with different flow rates, we cannot strictly compare the sensitivities of mesoporous layers with Al-ALD and microporous layers.

https://doi.org/10.1021/acsanm.2c02741
ACS Appl. Nano Mater. 2022, 5, 16126−16135

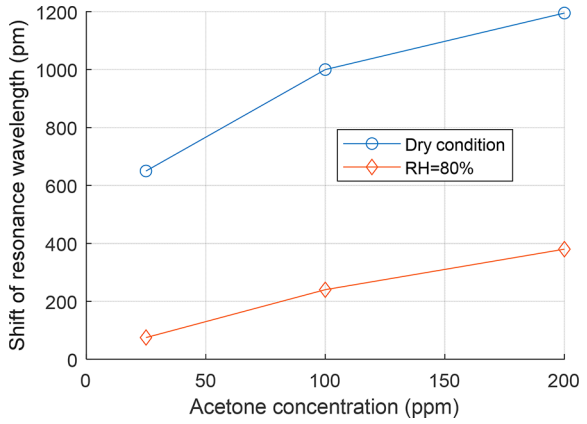

Figure 15. Resonance wavelength responses to different acetone concentrations at different relative humidity levels (80% and very low) at 20 °C.

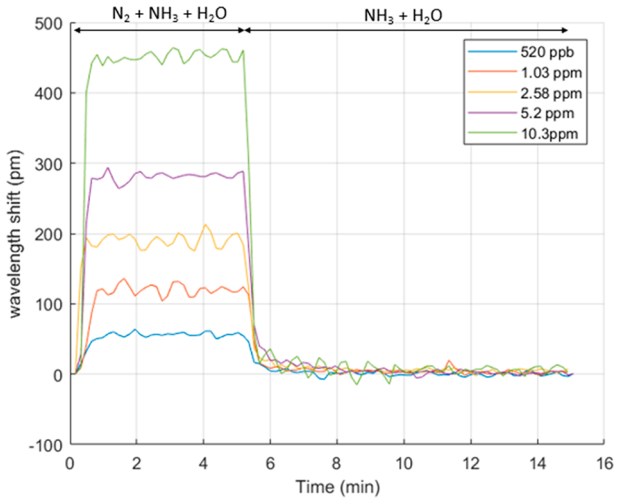

Figure 16. Resonance wavelength shifts of MRRs coated with mesoporous layer (pore size = 7 nm, 10-cycle Al-ALD) for different NH_3 concentrations.

CONCLUSIONS

Functional nanoporous films offer attractive features for selective and highly sensitive gas detection on nano/micro-photonic chips. Selective, fast and reversible, and reproducible NH_3 detection is demonstrated using acidic nanoporous silica–alumina films on silicon micro-ring resonators. Both microporous layers and mesoporous layers with Al-ALD demonstrated ppb level detection. A key mechanism behind reversible NH_3 sensitivity observed in our sensors is experimentally investigated. Sensitive, fast, and selective nanoporous film-coated sensors demonstrated here open new opportunities for portable and real-time gas sensing in medical and industrial applications.

AUTHOR INFORMATION

Corresponding Author

Sreeprasanth Pulinthanathu Sree − *Department of Materials Engineering, KU Leuven, 3001 Leuven, Belgium; Centre for Surface Chemistry and Catalysis, KU Leuven, 3001 Leuven, Belgium;* orcid.org/0000-0002-3464-5355; Email: sree.psree@kuleuven.be

Authors

Yanlu Li − *Photonics Research Group, Ghent University-imec, 9052 Gent, Belgium; Center for Nano- and Biophotonics, Ghent University, 9052 Ghent, Belgium*

Claudio Bellani − *Department of Materials Engineering, KU Leuven, 3001 Leuven, Belgium*

Nebiyu Yebo − *Photonics Research Group, Ghent University-imec, 9052 Gent, Belgium; Center for Nano- and Biophotonics, Ghent University, 9052 Ghent, Belgium*

Jolien Dendooven − *Department of Solid State Sciences, Ghent University, B-9000 Gent, Belgium;* orcid.org/0000-0002-2385-3693

Jin Won Seo − *Department of Materials Engineering, KU Leuven, 3001 Leuven, Belgium;* orcid.org/0000-0003-4937-0769

Christophe Detavernier − *Department of Solid State Sciences, Ghent University, B-9000 Gent, Belgium;* orcid.org/0000-0001-7653-0858

Roel Baets − *Photonics Research Group, Ghent University-imec, 9052 Gent, Belgium; Center for Nano- and Biophotonics, Ghent University, 9052 Ghent, Belgium*

Johan A. Martens − *Centre for Surface Chemistry and Catalysis, KU Leuven, 3001 Leuven, Belgium;* orcid.org/0000-0002-9292-2357

Complete contact information is available at: https://pubs.acs.org/10.1021/acsanm.2c02741

Author Contributions

The manuscript was written through the contributions of all authors.

Notes

The authors declare no competing financial interest.

ACKNOWLEDGMENTS

Y.L. and R.B. acknowledge the Industrieel Onderzoeksfonds Hoofdfinanciering (IOF) funding project BREAZE, JAM, RB, SPS, NAY and acknowledge the Flemish Government for long-term structural funding (Methusalem). These authors also acknowledge the European Research Council (ERC)-Inspectra project of RB for funding. C.D. acknowledges the Fonds voor Wetenschappelijke Onderzoek Vlaanderen (FWO) and the European Research Council (ERC) for funding. C.D. acknowledges the FWO-Vlaanderen for funding (Project G077012).

REFERENCES

(1) Cortial, G.; Siutkowski, M.; Goettmann, F.; Moores, A.; Boissière, C.; Grosso, D.; Le Floch, P.; Sanchez, C. Metallic Nanoparticles Hosted in Mesoporous Oxide Thin Films for Catalytic Applications. *Small* **2006**, *2* (8–9), 1042–1045.

(2) Kang, T.; Oh, S.; Hong, S.; Moon, J.; Yi, J. Mesoporous Silica Thin Films as a Spatially Extended Probe of Interfacial Electric Fields for Amplified Signal Transduction in Surface Plasmon Resonance Spectroscopy. *Chem. Commun.* **2006**, *28*, 2998.

(3) Walcarius, A.; Kuhn, A. Ordered Porous Thin Films in Electrochemical Analysis. *TrAC Trends Anal. Chem.* **2008**, *27* (7), 593–603.

(4) Monton, M. R. N.; Forsberg, E. M.; Brennan, J. D. Tailoring Sol–Gel-Derived Silica Materials for Optical Biosensing. *Chem. Mater.* **2012**, *24* (5), 796–811.

(5) Konjhodzic, D.; Schröter, S.; Marlow, F. Ultra-Low Refractive Index Mesoporous Substrates for Waveguide Structures. *Phys. status solidi* **2007**, *204* (11), 3676–3688.

(6) Kataoka, S.; Endo, A.; Harada, A.; Inagi, Y.; Ohmori, T. Characterization of Mesoporous Catalyst Supports on Microreactor Walls. *Appl. Catal. A Gen* **2008**, *342* (1−2), 107−112.
(7) Angelos, S.; Liong, M.; Choi, E.; Zink, J. I. Mesoporous Silicate Materials as Substrates for Molecular Machines and Drug Delivery. *Chem. Eng. J.* **2008**, *137* (1), 4−13.
(8) Martucci, A.; Buso, D.; Guglielmi, M.; Zbroniec, L.; Koshizaki, N.; Post, M. Optical Gas Sensing Properties of Silica Film Doped with Cobalt Oxide Nanocrystals. *J. Sol-Gel Sci. Technol.* **2004**, *32* (1−3), 243−246.
(9) Tang, X.; Provenzano, J.; Xu, Z.; Dong, J.; Duan, H.; Xiao, H. Acidic ZSM-5 Zeolite-Coated Long Period Fiber Grating for Optical Sensing of Ammonia. *J. Mater. Chem.* **2011**, *21* (1), 181−186.
(10) Yebo, N. A.; Lommens, P.; Hens, Z.; Baets, R. An Integrated Optic Ethanol Vapor Sensor Based on a Silicon-on-Insulator Microring Resonator Coated with a Porous ZnO Film. *Opt. Express* **2010**, *18* (11), 11859.
(11) Yebo, N. A.; Sree, S. P.; Levrau, E.; Detavernier, C.; Hens, Z.; Martens, J. A.; Baets, R. Selective and Reversible Ammonia Gas Detection with Nanoporous Film Functionalized Silicon Photonic Micro-Ring Resonator. *Opt. Express* **2012**, *20* (11), 11855.
(12) Antonacci, G.; Goyvaerts, J.; Zhao, H.; Baumgartner, B.; Lendl, B.; Baets, R. Ultra-Sensitive Refractive Index Gas Sensor with Functionalized Silicon Nitride Photonic Circuits. *APL Photonics* **2020**, *5* (8), 081301.
(13) Linares, N.; Serrano, E.; Rico, M.; Mariana Balu, A.; Losada, E.; Luque, R.; García-Martínez, J. Incorporation of Chemical Functionalities in the Framework of Mesoporous Silica. *Chem. Commun.* **2011**, *47* (32), 9024.
(14) Detavernier, C.; Dendooven, J.; Pulinthanathu Sree, S.; Ludwig, K. F.; Martens, J. A. Tailoring Nanoporous Materials by Atomic Layer Deposition. *Chem. Soc. Rev.* **2011**, *40* (11), 5242.
(15) Sree, S. P.; Dendooven, J.; Korányi, T. I.; Vanbutsele, G.; Houthoofd, K.; Deduytsche, D.; Detavernier, C.; Martens, J. A. Aluminium Atomic Layer Deposition Applied to Mesoporous Zeolites for Acid Catalytic Activity Enhancement. *Catal. Sci. & Technol.* **2011**, *1* (2), 218.
(16) Yebo, N. A.; Taillaert, D.; Roels, J.; Lahem, D.; Debliquy, M.; Van Thourhout, D.; Baets, R. Silicon-on-Insulator (SOI) Ring Resonator-Based Integrated Optical Hydrogen Sensor. *IEEE Photonics Technol. Lett.* **2009**, *21* (14), 960−962.
(17) Jokerst, N.; Royal, M.; Palit, S.; Luan, L.; Dhar, S.; Tyler, T. Chip Scale Integrated Microresonator Sensing Systems. *J. Biophotonics* **2009**, *2* (4), 212−226.
(18) Sun, Y.; Fan, X. Analysis of Ring Resonators for Chemical Vapor Sensor Development. *Opt. Express* **2008**, *16* (14), 10254.
(19) Nitkowski, A.; Chen, L.; Lipson, M. Cavity-Enhanced on-Chip Absorption Spectroscopy Using Microring Resonators. *Opt. Express* **2008**, *16* (16), 11930.
(20) Robinson, J. T.; Chen, L.; Lipson, M. On-Chip Gas Detection in Silicon Optical Microcavities. *Opt. Express* **2008**, *16* (6), 4296.
(21) Felix, S. P.; Savill-Jowitt, C.; Brown, D. R. Base Adsorption Calorimetry for Characterising Surface Acidity: A Comparison between Pulse Flow and Conventional "Static" Techniques. *Thermochim. Acta* **2005**, *433* (1−2), 59−65.
(22) Gomri, S.; Seguin, J.-L.; Guerin, J.; Aguir, K. A Mobility and Free Carriers Density Fluctuations Based Model of Adsorption−Desorption Noise in Gas Sensor. *J. Phys. D: Appl. Phys.* **2008**, *41* (6), 065501.
(23) Vallaey, B.; Radhakrishnan, S.; Heylen, S.; Chandran, C. V.; Taulelle, F.; Breynaert, E.; Martens, J. A. Reversible Room Temperature Ammonia Gas Absorption in Pore Water of Microporous Silica−Alumina for Sensing Applications. *Phys. Chem. Chem. Phys.* **2018**, *20* (19), 13528−13536.
(24) Liu, X.; Cheng, S.; Liu, H.; Hu, S.; Zhang, D.; Ning, H. A Survey on Gas Sensing Technology. *Sensors (Basel)* **2012**, *12* (7), 9635−9665.
(25) Timmer, B.; Olthuis, W.; Berg, A. van den. Ammonia Sensors and Their Applications—a Review. *Sensors Actuators B Chem.* **2005**, *107* (2), 666−677.
(26) Chang, S. C.; Stetter, J. R.; Cha, C. S. Amperometric Gas Sensors. *Talanta* **1993**, *40* (4), 461−477.
(27) Moseley, P. T. Progress in the Development of Semiconducting Metal Oxide Gas Sensors: A Review. *Meas. Sci. Technol.* **2017**, *28* (8), 082001.
(28) Abdulla, S.; Mathew, T. L.; Pullithadathil, B. Highly Sensitive, Room Temperature Gas Sensor Based on Polyaniline-Multiwalled Carbon Nanotubes (PANI/MWCNTs) Nanocomposite for Trace-Level Ammonia Detection. *Sensors Actuators B Chem.* **2015**, *221*, 1523−1534.
(29) Das, T. K.; Prusty, S. Review on Conducting Polymers and Their Applications. *Polym. Plast. Technol. Eng.* **2012**, *51* (14), 1487−1500.
(30) Pandey, S. Highly Sensitive and Selective Chemiresistor Gas/Vapor Sensors Based on Polyaniline Nanocomposite: A Comprehensive Review. *J. Sci. Adv. Mater. Devices* **2016**, *1* (4), 431−453.
(31) Mir, M. A.; Bhat, M. A.; Naikoo, R. A.; Bhat, R. A.; khan, M.; Shaik, M.; Kumar, P.; Sharma, P. K.; Tomar, R. Utilization of Zeolite/Polymer Composites for Gas Sensing: A Review. *Sensors Actuators B Chem.* **2017**, *242*, 1007−1020.
(32) Stassen, I.; Burtch, N.; Talin, A.; Falcaro, P.; Allendorf, M.; Ameloot, R. An Updated Roadmap for the Integration of Metal−Organic Frameworks with Electronic Devices and Chemical Sensors. *Chem. Soc. Rev.* **2017**, *46* (11), 3185−3241.
(33) Petit, C.; Bandosz, T. J. MOF-Graphite Oxide Composites: Combining the Uniqueness of Graphene Layers and Metal-Organic Frameworks. *Adv. Mater.* **2009**, *21* (46), 4753−4757.
(34) Peng, N.; Zhang, Q.; Chow, C. L.; Tan, O. K.; Marzari, N. Sensing Mechanisms for Carbon Nanotube Based NH_3 Gas Detection. *Nano Lett.* **2009**, *9* (4), 1626−1630.
(35) Sharma, S.; Hussain, S.; Singh, S.; Islam, S. S. MWCNT-Conducting Polymer Composite Based Ammonia Gas Sensors: A New Approach for Complete Recovery Process. *Sensors Actuators B Chem.* **2014**, *194*, 213−219.
(36) Rigoni, F.; Tognolini, S.; Borghetti, P.; Drera, G.; Pagliara, S.; Goldoni, A.; Sangaletti, L. Enhancing the Sensitivity of Chemiresistor Gas Sensors Based on Pristine Carbon Nanotubes to Detect Low-Ppb Ammonia Concentrations in the Environment. *Analyst* **2013**, *138* (24), 7392.
(37) Septiani, N. L. W.; Yuliarto, B. Review—The Development of Gas Sensor Based on Carbon Nanotubes. *J. Electrochem. Soc.* **2016**, *163* (3), B97−B106.
(38) Zaporotskova, I. V.; Boroznina, N. P.; Parkhomenko, Y. N.; Kozhitov, L. V. Carbon Nanotubes: Sensor Properties. A Review. *Mod. Electron. Mater.* **2016**, *2* (4), 95−105.
(39) Varghese, S. S.; Lonkar, S.; Singh, K. K.; Swaminathan, S.; Abdala, A. Recent Advances in Graphene Based Gas Sensors. *Sensors Actuators B Chem.* **2015**, *218*, 160−183.
(40) Chen, G.; Paronyan, T. M.; Harutyunyan, A. R. Sub-Ppt Gas Detection with Pristine Graphene. *Appl. Phys. Lett.* **2012**, *101* (5), 053119.
(41) Jiang, X.; Qavi, A. J.; Huang, S. H.; Yang, L. Whispering-Gallery Sensors. *Matter* **2020**, *3* (2), 371−392.
(42) Armani, D. K.; Kippenberg, T. J.; Spillane, S. M.; Vahala, K. J. Ultra-High-Q Toroid Microcavity on a Chip. *Nature* **2003**, *421* (6926), 925−928.
(43) Lee, H.; Chen, T.; Li, J.; Yang, K. Y.; Jeon, S.; Painter, O.; Vahala, K. J. Chemically Etched Ultrahigh-Q Wedge-Resonator on a Silicon Chip. *Nat. Photonics* **2012**, *6* (6), 369−373.
(44) Xu, Q.; Schmidt, B.; Pradhan, S.; Lipson, M. Micrometre-Scale Silicon Electro-Optic Modulator. *Nature* **2005**, *435* (7040), 325−327.
(45) Gondarenko, A.; Levy, J. S.; Lipson, M. High Confinement Micron-Scale Silicon Nitride High Q Ring Resonator. *Opt. Express* **2009**, *17* (14), 11366.
(46) Li, C.; Lohrey, T.; Nguyen, P.-D.; Min, Z.; Tang, Y.; Ge, C.; Sercel, Z. P.; McLeod, E.; Stoltz, B. M.; Su, J. Part-per-Trillion Trace

https://doi.org/10.1021/acsanm.2c02741
ACS Appl. Nano Mater. 2022, 5, 16126−16135

Selective Gas Detection Using Frequency Locked Whispering-Gallery Mode Microtoroids. *ACS Appl. Mater. Interfaces* **2022**, *14*, 42430.
(47) Schmidt, S.; Flueckiger, J.; Wu, W.; Grist, S. M.; Fard, S. T.; Donzella, V.; Khumwan, P.; Thompson, E. R.; Wang, Q.; Kulik, P.; Wang, X.; Sherwali, A.; Kirk, J.; Cheung, K. C.; Chrostowski, L.; Ratner, D.Improving the Performance of Silicon Photonic Rings, Disks, and Bragg Gratings for Use in Label-Free Biosensing. *Proceedings Volume 9166: Biosensing and Nanomedicine VII*; SPIE, 2014; pp 71−108; DOI: 10.1117/12.2062389.
(48) Selvaraja, S. K.; Jaenen, P.; Bogaerts, W.; Van Thourhout, D.; Dumon, P.; Baets, R. Fabrication of Photonic Wire and Crystal Circuits in Silicon-on-Insulator Using 193-Nm Optical Lithography. *J. Light. Technol.* **2009**, *27* (18), 4076−4083.
(49) Sree, S. P.; Dendooven, J.; Smeets, D.; Deduytsche, D.; Aerts, A.; Vanstreels, K.; Baklanov, M. R.; Seo, J. W.; Temst, K.; Vantomme, A.; Detavernier, C.; Martens, J. A. Spacious and Mechanically Flexible Mesoporous Silica Thin Film Composed of an Open Network of Interlinked Nanoslabs. *J. Mater. Chem.* **2011**, *21* (21), 7692.
(50) Baklanov, M. R.; Mogilnikov, K. P.; Polovinkin, V. G.; Dultsev, F. N. Determination of Pore Size Distribution in Thin Films by Ellipsometric Porosimetry. *J. Vac. Sci. & Technol. B Microelectron. Nanom. Struct* **2000**, *18* (3), 1385.
(51) Aguilar, A. D.; Forzani, E. S.; Nagahara, L. A.; Amlani, I.; Tsui, R.; Tao, N. J. A Breath Ammonia Sensor Based on Conducting Polymer Nanojunctions. *IEEE Sens. J.* **2008**, *8* (3), 269−273.
(52) Heiduschka, P.; Preschel, M.; Rösch, M.; Göpel, W. Regeneration of an Electropolymerised Polypyrrole Layer for the Amperometric Detection of Ammonia. *Biosens. Bioelectron* **1997**, *12* (12), 1227−1231.

https://doi.org/10.1021/acsanm.2c02741
ACS Appl. Nano Mater. 2022, 5, 16126−16135